energy&fuels

pubs.acs.org/EF Article

Shale Oil Potential and Mobility of Low-Maturity Lacustrine Shales: Implications from NMR Analysis in the Bohai Bay Basin

Di Chen, Xiongqi Pang,* Fujie Jiang,* Guoyong Liu, Zhihong Pan, and Yang Liu

Cite This: *Energy Fuels* 2021, 35, 2209−2223

Read Online

ACCESS | Metrics & More | Article Recommendations

Downloaded via UNIV OF CONNECTICUT on May 15, 2021 at 13:41:55 (UTC).
See https://pubs.acs.org/sharingguidelines for options on how to legitimately share published articles.

ABSTRACT: A vital factor influencing shale oil exploration in lacustrine shale reservoirs is oil mobility, which is closely associated with the shale pore structure and fluid properties, especially for the low-maturity lacustrine shales in China. In this study, the oil mobility and shale oil potential in the Middle Eocene Shahejie Formation lacustrine shales (MES shales) of the Nanpu Sag in the Bohai Bay Basin are evaluated by using nuclear magnetic resonance (NMR) experiments. The low-maturity MES shales have low porosity with NMR porosity ranging from 4.29−7.41%, and the oil saturation ranges from 9.35−36.09%. The pore types are various including intergranular and dissolution pores and fractures. The pore space size spans the range from nano- to microscale, and they are predominantly mesopres. The pore structure for fluid flow is complex and has good self-similarity with high fractal dimensions. The abundant brittle minerals with a relatively high brittleness index value benefit the fracturing of MES shales. Due to the high viscosity and heavy oil in low-maturity shales, bulk relaxation is proposed to analyze the oil properties in this study. The oil viscosity of MES shales mainly ranges from 2 to 70 cP. The movable oil with a viscosity lower than 10 cP accounts for 53.66% of the total oil-filling pore space. For the black mud-shales dominating MES shales, the thermal maturity influences the porosity, viscosity, free hydrocarbon content, and oil saturation in the rocks. Higher thermal maturity would facilitate pore space development with higher porosity, enhance the free hydrocarbon content and oil saturation, and reduce the oil viscosity to some extent. Moreover, MES shales have geological conditions similar to and better brittleness than those of other shale oil producing areas, which further supports the considerable and promising shale oil potential in this formation, especially for deposits located in deeper positions of the Nanpu Sag. The technologies of in situ conversion process and hydraulic fracturing make the resource potential of shale oil in the Nanpu Sag more attractive.

1. INTRODUCTION

As world's energy demand increases, shale oil resources have attracted increasing attention.[1−4] Oil mobility is critical for the assessment of shale oil resource and development, especially for lacustrine shale oil resources.[5,6] However, few studies have focused on the oil mobility in lacustrine shales. Shale oil exploration has generated promising results in China, while the thermal maturity of the targeted shales is commonly low.[7−10] The study of oil mobility in low-maturity shales is essential for identifying production "sweet spots".

The oil mobility in shale reservoirs is closely related to the composition of minerals and organic matter (OM) as well as its complex pore structure, thermal maturity, liquid properties, and formation pressure and temperature.[2,5,6,11−15] The main existing methods focus on molecular dynamics simulation, organic geochemistry, and nuclear magnetic resonance (NMR).[5,6,16−22] Molecular dynamics simulation provides a theoretical research approach to microscopically simulate fluid molecule adsorption, flow, and properties in porous materials.[19,23−25] However, this method is time-consuming, and its simulated results are difficult to verify against the actual geological situation. The organic geochemical method for evaluating liquid mobility in shale sediments relies on key geochemical parameters obtained from laboratory experiments.[6,10,13] This method can reflect the amounts of movable liquids and is relatively reliable for evaluating shale oil resources. However, it cannot present the state and distribution of liquids in the complex pore system intuitively and directly, nor does it consider the subsurface liquid properties and geological conditions.[7,26−28] In contrast, NMR is a noninvasive technique that can provide information about the pore structure, liquid properties, oil saturation, in situ fluid amount, and interactions between pore fluids and rock.[17,29] This approach has been widely used to characterize the pore structure and pore size distribution in tight reservoirs.[17,18,30−35] However, most NMR studies on fluid mobility were mainly conducted under water-saturated and fully centrifuged conditions, which reflects water mobility but does not represent oil mobility directly due to its different physicochemical properties. Moreover, few NMR studies have been carried out to determine the oil saturation and properties as well as the oil distribution in pore system of shales. However, these variables are imperative for the further exploration of shale oil resources.

Received: November 24, 2020
Revised: January 9, 2021
Published: January 15, 2021

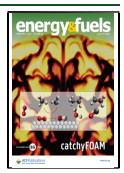

ACS Publications © 2021 American Chemical Society

https://dx.doi.org/10.1021/acs.energyfuels.0c03978
Energy Fuels 2021, 35, 2209−2223

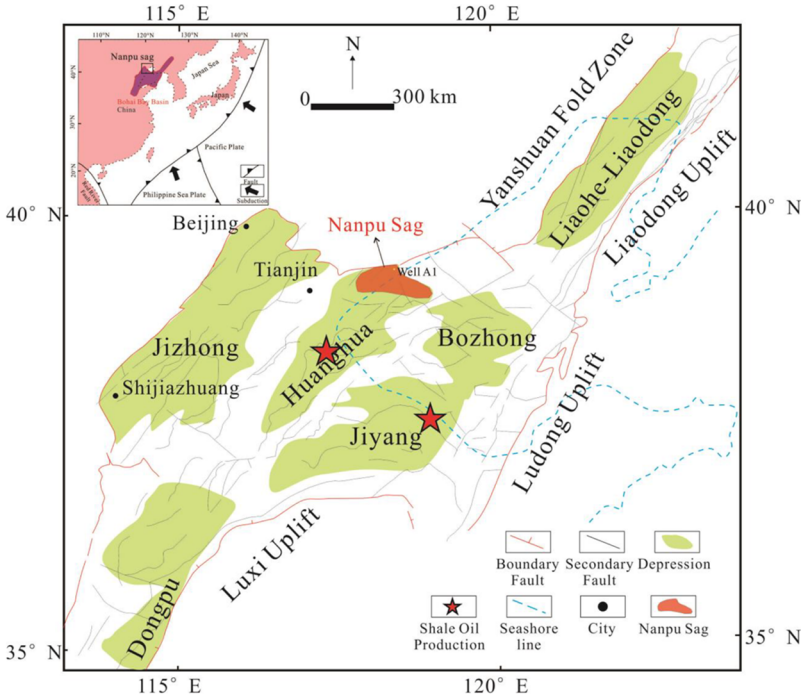

Figure 1. Geological location of the Nanpu Sag in the Bohai Bay Basin.

In this study, low-field NMR combined with microscopy observations and geochemical experiments were performed on the low-maturity Eocene lacustrine shales in the Nanpu Sag of the Bohai Bay Basin with three objectives: (1) investigating the pore structure and pore size distribution in the Eocene lacustrine shales, (2) analyzing the oil properties and mobility in the low-maturity shales, and (3) estimating the shale oil potential in the Nanpu Sag.

2. GEOLOGICAL SETTING

The Bohai Bay Basin is a Mesozoic−Cenozoic oil-bearing rift basin on the eastern Asian continent and has produced abundant oil/gas in recent decades[36] (Figure 1). Massive terrestrial sediments cover the Mesozoic and pre-Mesozoic basement rocks of the Bohai Bay Basin[37] (Figure 2). The increased difficulty with conventional resource exploration and the increased oil and gas demand in China have spurred unconventional oil/gas resource exploration in the Bohai Bay Basin, especially for shale oil resources.[6,38,39] To date, good shale oil deposits have been discovered in Eocene shale sediments of the Bohai Bay Basin with high daily production, such as in the Zhanhua and Dongying Sags.[38,40,41] Moreover, a breakthrough in shale oil exploration has been attained in the Cangdong Sag with commercial shale oil flow.[39] The Nanpu Sag adjoins the Guandong, Zhanhua, and Dongying Sags, has similar geological conditions, and is an important hydrocarbon-producing sag in the Bohai Bay Basin[37] (Figure 1). Constrained by the sea, deep shale oil resource exploration in the Nanpu Sag has faced many difficulties in recent years. The Gaoliu area of the Nanpu Sag has a suitable oil occurrence in the MES shale sediments. Although the MES shales are thin, they are one of the most important source rocks in the Nanpu Sag, contributing a large volume of oil and gas resources in conventional traps.[9] The MES shales were deposited in semideep and deep lacustrine environments and are dominated by black shales and gray-black mudstones with abundant organic matter[9,37] (Figure 2). The MES shales here are typically low maturity, with vitrinite reflectance less than 0.7%.[9,42] Although MES shales have good hydrocarbon potential, few studies have been carried out on their pore structure and oil mobility. Recently, the A1 well in the Gaoliu area was successfully drilled in a complete suite of MES shale sediments with a 10 m layer of good oil occurrence. This finding is very encouraging and enhances the confidence in the shale oil exploration in the Nanpu Sag. A suite of continuous MES shale core samples were collected from the A1 well to analyze the pore structure and estimate the shale oil mobility as well as their vertical variation.

3. NMR THEORETICAL BACKGROUND

NMR refers to the response of atomic nuclei to a magnetic field.[17] Due to the net magnetic moment and angular momentum or spin, atomic nuclei which have an odd number of protons, neutrons, or both proceed to spin under a given magnetic field and the gravitational field of Earth.[17] When another external magnetic field is generated, the amplitude of these spinning magnetic nuclei will decay and produce irreversible rephrasing, thus inducing measurable resonant signals.[17] The external magnetic field often uses the CPMG sequence (invented by Carr, Purcell, Meiboom, and Gill),[17] which will produce transverse magnetization decay signals with transverse relaxation time (T_2). Because it is less time-consuming, the T_2 transverse relaxation is often preferentially measured in the laboratory.[18,34,35]

For the transverse relaxation, three relaxation mechanisms affect the fluids in rocks:[17,43] (1) bulk relaxation in connection with the intrinsic fluid properties, (2) surface relaxation reflecting the characteristics of the interaction between fluids and the solid grain interfaces, and (3) diffusion relaxation induced by the gradient field. These relaxation processes act in parallel, and their rates are additive. For a water-wet rock, the relaxation of water is dominated by the surface relaxation

https://dx.doi.org/10.1021/acs.energyfuels.0c03978
Energy Fuels 2021, 35, 2209−2223

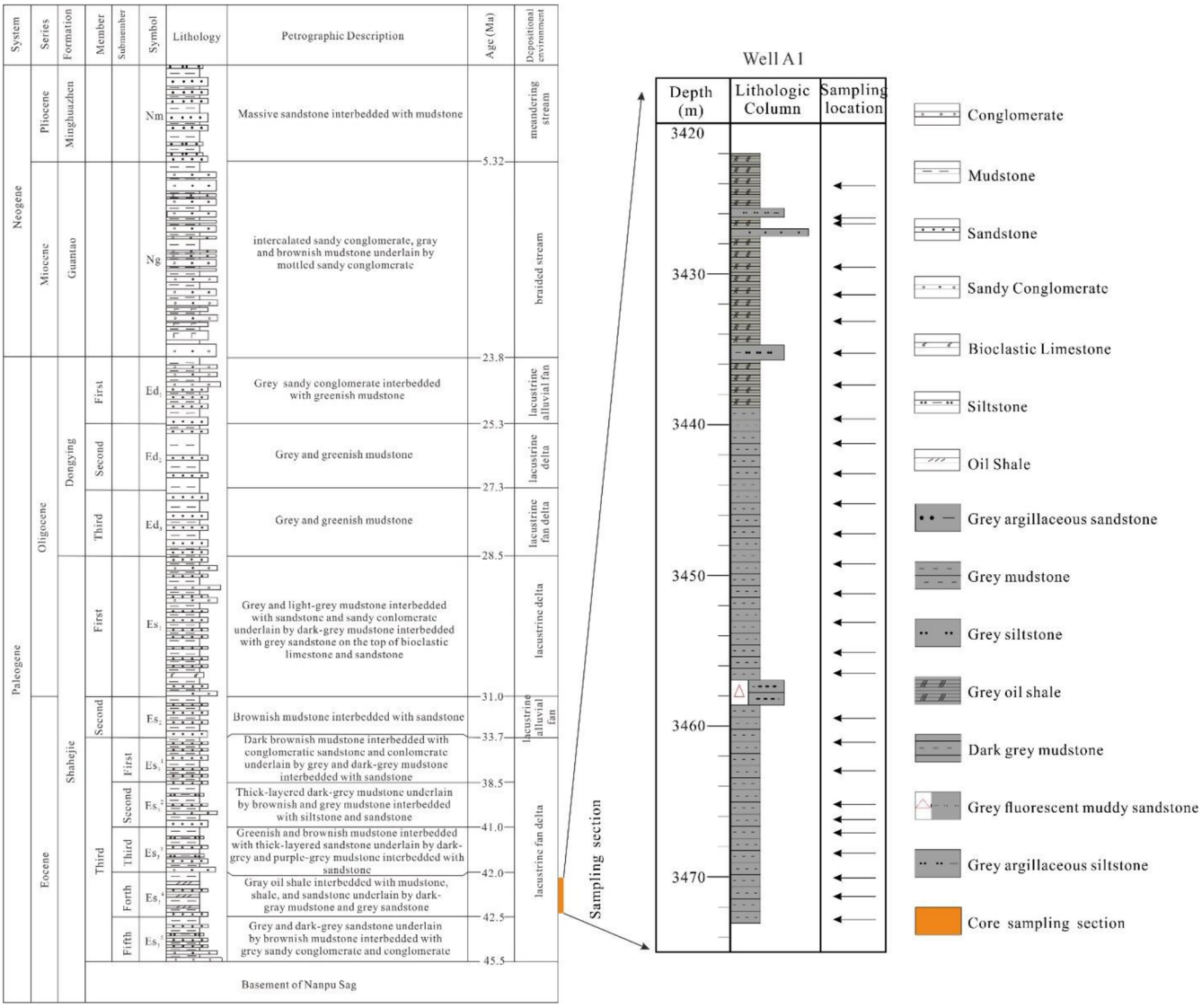

Figure 2. Stratigraphy distribution modified from Dong et al.[37] and Chen et al.[9] and the sampling location in this study.

mechanism, while the relaxation of oil is dominated by bulk relaxation, especially for high-viscosity oil and that in larger pore space or cracks.[17] In contrast, the occurrences of oil and water will be reversed in the strongly oil-wet rock. Fine grains are significant barriers to diffusion, and diffusion relaxation would decrease under a low and uniform magnetic field.[17,18,43,44] Therefore, for the water in a water-wet rock under a homogeneous magnetic field and CPMG sequence, only surface relaxation need be considered.

For the bulk relaxation mechanism, the oil T_2 relaxation time is associated with the temperature and fluid viscosity, and the relationship is as follows:

$$T_{2\text{bulk}} = 0.00713 \times \frac{T_K}{\eta} \tag{1}$$

where T_K is the Kelvin temperature (K) and η is the viscosity (cP). For the surface relaxation mechanism, the relaxation time is the average relaxation time for the nuclei in all pores.[17,30] The nuclei in small pores more easily interact with the grain surface than those in larger pores. Therefore, the shorter relaxation time could reflect the smaller pores.[17,30] The rates of relaxation are generally related to surface relaxation and pore surface-to-volume ratio, and this relationship can be described as[17,30]

$$\frac{1}{T_2} = \rho \frac{S}{V} \tag{2}$$

where T_2 is the transverse relaxation time resulting from surface relaxation (in seconds) and ρ is the surface relaxivity (in micrometers/second), which is related to the concentration of paramagnetic sites on pore walls and reflects the ability of pore walls to promote proton relaxation. S/V is the surface area-to-volume ratio (per micrometer). For simple shapes, the surface-to-volume ratio is $3/r$, where r is the radius of the sphere.[17] For complex shapes, the shape factor F_p will be used to describe the surface-to-volume ratio as[35]

$$\frac{S}{V} = \frac{F_p}{r} \tag{3}$$

Then, the relationship between the pore size and NMR transverse relaxation time T_2 can be described as

https://dx.doi.org/10.1021/acs.energyfuels.0c03978
Energy Fuels 2021, 35, 2209−2223

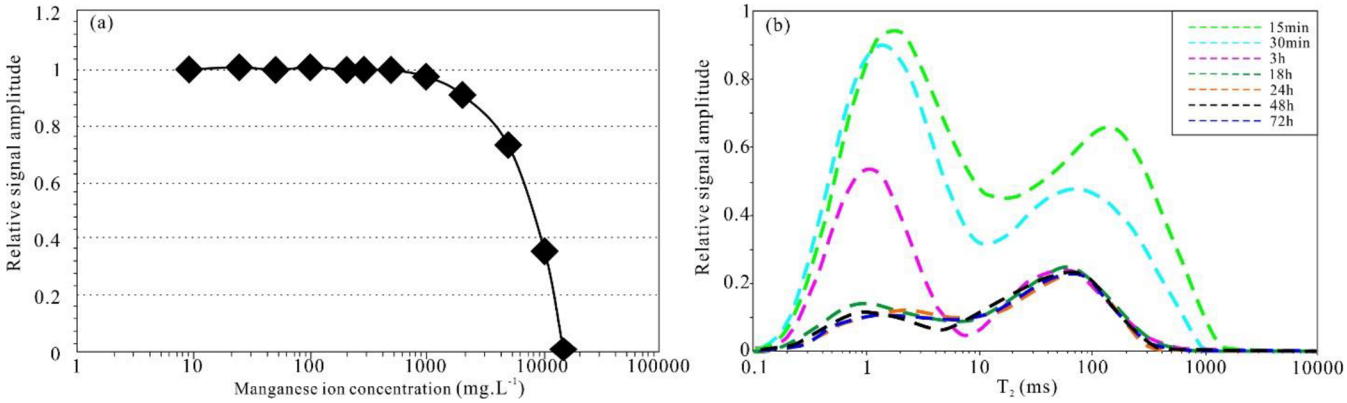

Figure 3. Shielding effect of manganese ion on the NMR signals.[46] (a) A better shielding effect is found with higher manganese ion concentration. (b) Manganese has a stable shielding effect on NMR signals after 18 h at the same concentration of manganese ion.

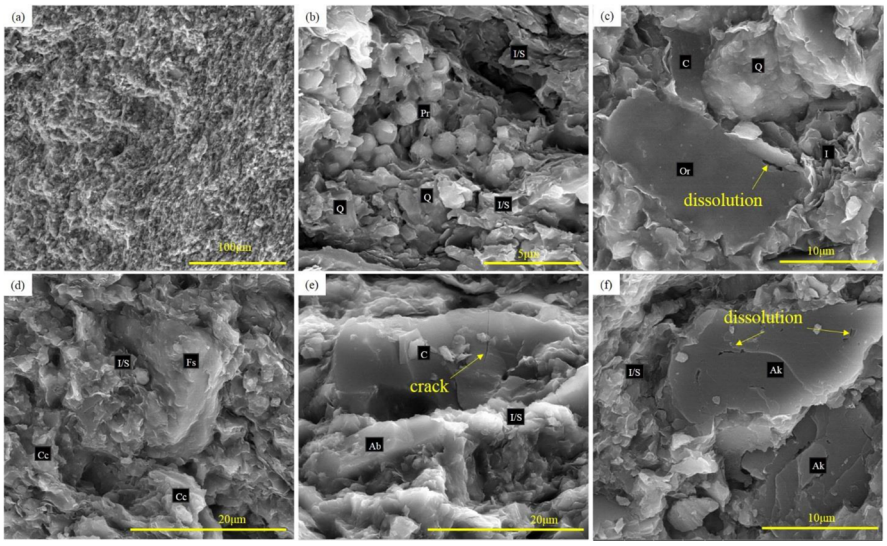

Figure 4. Morphological images from SEM observation for MES shales. Many minerals can be observed, including quartz (Q), pyrite (Pr), Illite (I), illite/smectite mixture (I/S), orthoclase (Or), calcite (Cc), feldspar (Fs), albite (Ab), ankerite (Ak), and OM (C). Some cracks and dissolution can also been observed.

$$r = \rho \times F_p \times T_2 \quad (4)$$

If the surface relaxivity can be determined, then the NMR T_2 spectrum can be used to quantitatively characterize the pore size distribution in rocks. The surface relaxivity largely varies with the mineralogy.[14,36] Carbonate surfaces exhibit a lower surface relaxivity than that of quartz surfaces, and high-iron rocks have a higher surface relaxivity.[14]

In addition to reflecting pore information and providing an accurate estimate of the pore size distribution, NMR relaxation time distributions can also be used to analyze the oil information in porous media.[17,29,45] To characterize the oil saturation in cores containing oil and water, the signals produced by water need to be filtered out. Paramagnetic ions can cover the resonant signals from water.[45] If the manganese ion concentration is high enough, then the T_2 of water could be reduced to below the dead time, and the water signal would disappear. However, manganese does not dissolve in hydrocarbons. Therefore, T_2 from hydrocarbons is unaffected, and its signal remains. Figure 3a shows that the signal intensity disappears when the concentration of manganese ions is higher than 10 000 mg/L.[46] In addition, the signal intensity of the core sample containing oil and water remains stable after immersion in a manganese solution with the same concentration for 18 h[46] (Figure 3b).

4. SAMPLING AND METHODS

The sampling section of well A1 ranges from 3424.13 to 3472.83 m. The lithologies of the MES shales are mainly dark gray mudstones, gray oil shales, and interbedded gray argillaceous siltstones. In this study, 28 relatively good oil-bearing MES shale samples were collected to conduct NMR and scanning electron microscopy (SEM) experiments to analyze the mineral characteristics, pore structure, oil-bearing features and oil mobility.

Before the NMR experiments, horizontal cylindrical core plugs (2.5 cm in diameter and 4 cm length) were cut from the MES samples. All the MES shale samples in this study were subjected to two suites of NMR experiments. One suite was performed to obtain oil signals with which to characterize the oil-containing pore space. For this suite, all collected samples were immersed in a solution with a manganese ion concentration of 15 000 mg/L and incubated for 24 h to ensure that the water signal was effectively suppressed. For the other suite of experiments, all core plugs were completely immersed in a 3% potassium chloride brine solution at 35 MPa under vacuum for 24 h to ensure that the samples were fully saturated with brine and reduce the sensitivity effect of clay minerals. This suite of experiments was

https://dx.doi.org/10.1021/acs.energyfuels.0c03978
Energy Fuels 2021, 35, 2209−2223

executed to acquire the bulk signals corresponding to the bulk pore space.

The NMR measurements were performed with an AniMR-150 magnetic resonance imaging system at 35 °C. The instrument contains a permanent magnet with a magnetic field strength of 0.3 ± 0.05 T, and the resonance frequency is 2−30 MHz with an accuracy of 0.1 Hz. In this study, the CPMG sequence was applied in all corresponding experiments to obtain the distribution of the T_2 relaxation time. The measurement procedure settings were as follows: echo spacing, 0.1098 ms; echo number, 4096; and scan number, 64. The decay signals were detected and converted to T_2 distribution by using multiexponential fitted inversion.[17] The signal intensity distribution of the T_2 relaxation time was obtained by using the echo data with preset times and plotted in logarithmic space from 0.01 ms to 10 s. If the samples were saturated enough, then the pore space could be regarded as fully filled by brine or oil in the two sets experiments, and the measured magnitude of the transverse magnetization could reflect the brine-filled pore volume and oil-filled pore volume, respectively. In this study, the signal intensity was converted into the porosity through comparison with a preset standard sample by using the area proportion. The bulk and oil-containing porosities were calculated according to the intensity of the brine and oil signals, respectively.[17] The NMR results are presented as curves of the incremental and cumulative porosities with the T_2 relaxation time.

To further characterize the minerals and pore spaces, we conducted SEM analysis of the MES samples. Freshly fractured surfaces were selected from among the broken samples and coated with a thin gold layer. The prepared samples were examined with a ZEISS Crossbeam 540 scanning electron microscope equipped with an energy-dispersive X-ray spectrometer. In addition, the components of the extracts were extracted with chloroform using a YS multifunction automatic extractionmeter. Dry powdered samples were encased in extracted filter paper, placed in the extracting barrel, and then doused with 1/2−2/3 volume of chloroform. Samples determined to be acceptable under three classes of fluoroscope before extraction were then heated for concentration and drying. The chloroform extraction results are expressed in weight percent (wt %). The mineral content, pyrolysis data, vitrinite reflectance (R_o), and TOC content used in this study are based on a previous study.[9] All experiments in this study were performed at the State Key Laboratory of Petroleum Resources and Prospecting in China.

5. RESULTS

5.1. Morphology of the MES Shales. The morphology of the pores and minerals in the MES shales are suitably characterized by SEM, as shown in Figure 4. The SEM images reveal that the pore size in the MES shales ranges from 4 to 19 μm (Figure 4a), and the pores exhibit lamellar structures that promote fluid flow. Pores are filled with granular pyrite, sheetlike mixed illite/smectite, and clean quartz (Figure 4b). Abundant OM could be observed in SEM (Figures 4c,e) surrounded by quartz, sheetlike illite, and orthoclase (Figure 4c). Cracks are observed in OM, which may be the result of hydrocarbon generation (Figure 4e). Dissolution phenomena are observed on the particle surfaces of quartz, orthoclase, calcite, albite, and ankerite, as shown in Figure 4, indicating that the MES shales were deposited under an acidic environment. The present pores include primary intergranular pores, intergranular and intragranular dissolution pores, microcracks in the OM, and micropores among the clay minerals.

According to the previous study,[9] the minerals in the MES shales are dominated by clays, with an average content of 42.75%, followed by quartz ranging from 10 to 34% (avg 21.73%) and calcite (2−39%, avg 17.28%). In addition, gypsum, halite, anhydrite, pyrite, and siderite were detected in the MES shales. Furthermore, the brittleness index (BI) could be calculated to assess the mechanical fracturing. Considering the abundant OM and plastic clays in lacustrine shales, this study calculates the BI by[47]

$$\mathrm{BI} = \frac{(V_{\mathrm{felsic}} + V_{\mathrm{carbonate}})}{(V_{\mathrm{clay}} + V_{\mathrm{felsic}} + V_{\mathrm{carbonate}} + V_{\mathrm{organic}})} \times 100 \quad (5)$$

where V_{felsic} is the felsic portion (%), $V_{\mathrm{carbonate}}$ is the carbonate portion (%), V_{clay} is the clay portion (%), and V_{organic} is the organic portion (%). When BI is >40%, the rock will be brittle; when BI is >60%, the rock is predicted to be highly brittle.[48] The BI of MES shales ranges from 37.73 to 79.36% (avg 55.80%, Figure 5), indicating good brittleness. Using eq 5, the calculated BI values of MES shales in the Nanpu Sag are higher than those of middle Jurassic Shimengou shales in the Qaidam Basin,[28] but they are slightly lower than those of Eocene shale sediments in the Dongying Sag[49] (Figure 5).

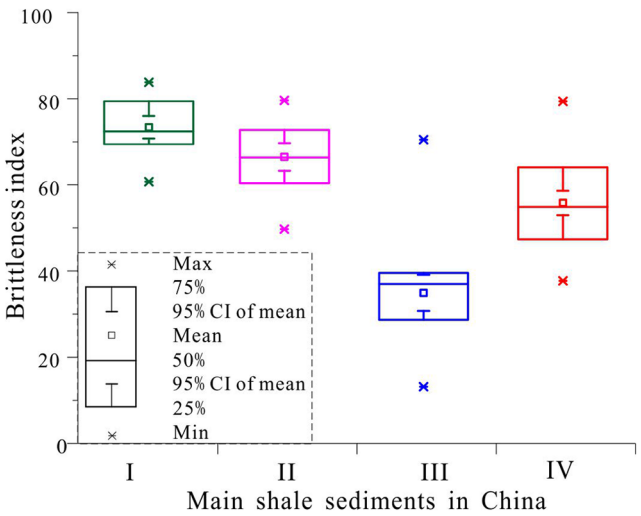

Figure 5. BI comparison among main lacustrine shale oil reservoirs in China. I represents the Paleogene shale sediments in the Jiangsu Basin and Jiyang Depression.[47] II and III represent the Eocene shale sediments in the Dongying Sag[66] and the middle Jurassic Shimengou shales in the Qaidam Basin,[28] respectively. IV represents the MES shales in this study.

5.2. NMR T_2 Distribution. All 28 MES shale samples were subjected to NMR measurements under brine- and manganese-saturated conditions. The distributions of the measured brine and oil information with the T_2 relaxation time, hereinafter referred to as BPD and OPD, respectively, are shown in Figure 6a,b. The T_2 relaxation times of the MES shales range from 0.02 to 30.20 ms in both BPD and OPD. All of the MES shale samples exhibit distinct bimodal distributions and contain two peaks for BPD and OPD, suggesting two relatively independent systems in the MES shales. The signal intensity of brine is notably higher than that of oil for all MES shale samples. In this study, certain parameters are used to quantitatively characterize the distributions. As shown in Figure 6a,b, T_{B1max}, T_{B2max}, T_{O1max}, and T_{O2max} are the T_2 relaxation times at the first and second peaks of BPD and OPD, respectively. Their typing could reflect fluid properties such as density and viscosity.[17,45] T_{B0} and T_{O0} are the final T_2 relaxation times of the first wave for BPD and OPD, respectively. T_{B0} could be regarded as the boundary between

https://dx.doi.org/10.1021/acs.energyfuels.0c03978
Energy Fuels 2021, 35, 2209−2223

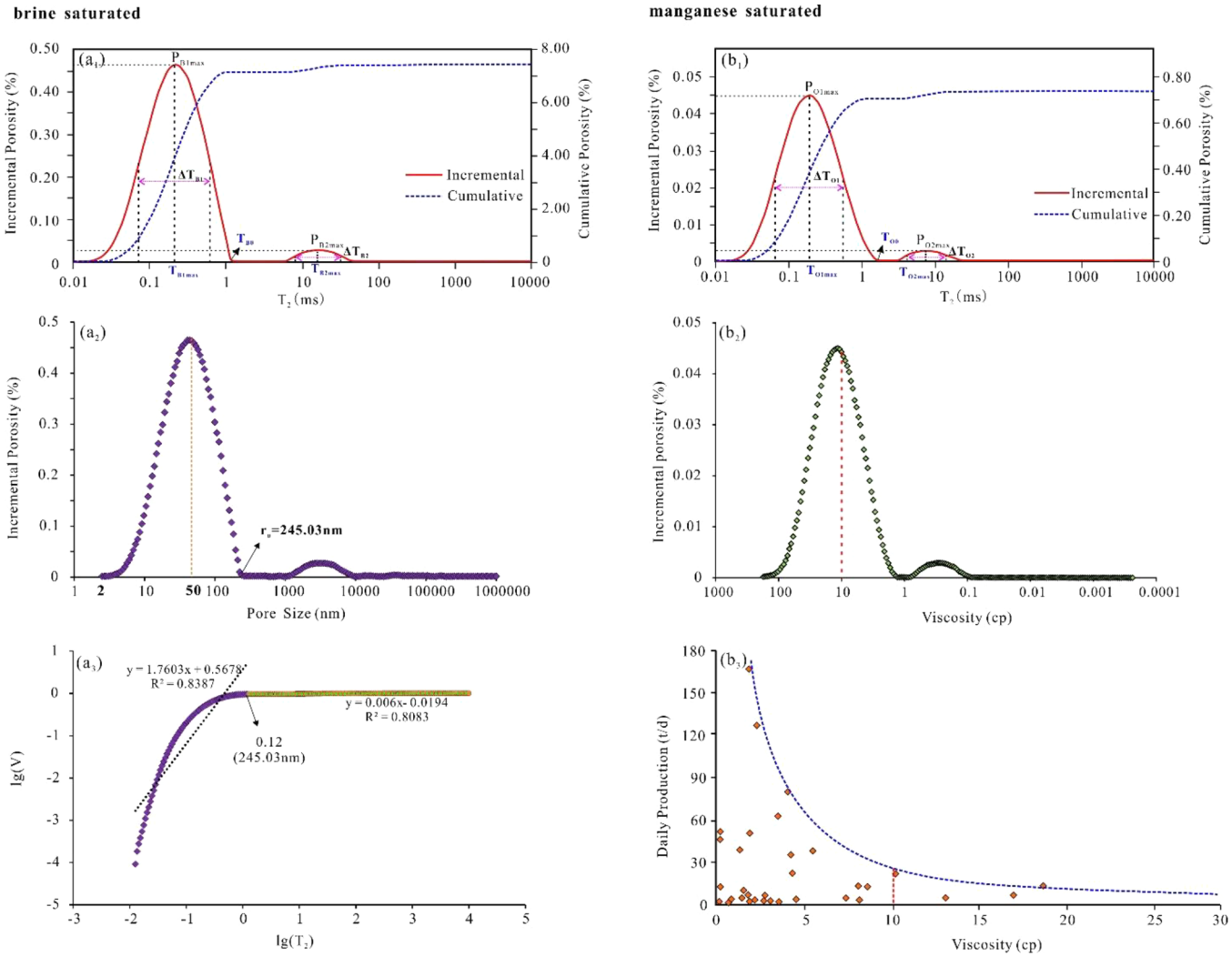

Figure 6. Results of two sets of NMR experiments of sample G-27. The other 27 samples show similar T_2 distribution. (a_1) Brine T_2 distribution. (a_2) Pore size distribution transformed from the T_2 distribution. (a_3) Calculation of fractal dimensions. Two suits of fractal dimensions could be discerned with a boundary at 245.03 nm corresponding to the pore size boundary between immovable and movable fluids (r_0). (b_1) Oil T_2 distribution under manganese-saturated conditions. (b_2) Oil viscosity distribution explained by bulk relaxation. (b_3) Relation of shale oil daily production and oil viscosity in the Jiyang Depression.[21] The red dotted lines shows the oil viscosity of 10 cP. The oil viscosity less than 10 cP has an acceptable daily production of shale oil in the Dongying Sag.

the movable and immovable fluids in this study according to the Coates model.[17,30,34] ΔT_{B1}, ΔT_{B2}, ΔT_{O1}, and ΔT_{O2} are the T_2 values differences of the half-peaks for BPD and OPD (Figure 6a,b), which could reflect the breadth of the signals. The parameters of the 28 MES shale samples are summarized in Table 1.

For most of the MES shale samples, T_{B1max} and T_{B2max} values are slightly larger than T_{O1max} and T_{O2max} values, respectively (Figure 7a). This finding indicates the relatively obvious position features of heavy oil in the water-wet rocks, and implies that the oil in MES shales is relatively heavy.[17] The BPD ΔT values are slightly higher than OPD ΔT values, showing a relatively narrow breadth in OPD (Figure 7b). This characteristic is consistent with oil in water-wet rock.[17] The BPD T_0 values have been regarded as the boundary of different pore systems,[17] but they have a disordered relation with OPD T_0 values for MES shales (Figure 7c). Three reasons may lead to this situation: (1) the complex pore systems and vertical anisotropy in the MES shales, (2) the large difference between the anisotropic fluid properties, and (3) the different relaxation mechanisms for the brine and oil. However, the proportion of immovable fluids is notably larger than that of movable fluids for bulk liquids in the MES shales.

5.3. Pore Size Distribution in the MES Shales. Equation 3 shows that the T_2 relaxation time can be converted into the pore size if the shape factor and surface relaxivity can be determined. For the MES shales in this study, the pore shape could be regarded as a sphere, and the value of F_p could be set as 3, for two reasons: (1) The clear bimodal T_2 relaxation distribution indicates two relatively independent pore systems coexisting in the MES shales, with a relatively low connectivity among pores. (2) The immovable fluids account for a larger percentage in the MES shales, also indicating a poor connectivity. These reasons suggest that there are very few pore throats in the MES shales and that the pores are relatively isolated.

Previous studies show that the surface relaxivity is strongly associated with minerals.[17,50] Here, minerals were considered as the only factor affecting surface relaxivity. Therefore, a quantitative relation to calculate surface relaxivity was fitted by

https://dx.doi.org/10.1021/acs.energyfuels.0c03978
Energy Fuels 2021, 35, 2209−2223

Table 1. Information on MES Shales and the Parameters Related to NMR Experiments

sample no.	depth (m)	surface relaxivity (μm/s)	T_{B1max} (ms)	T_{B2max} (ms)	T_{B0}	r_0 (nm)	T_{O1max} (ms)	T_{O2max} (ms)	T_{O0} (ms)	NMR porosity (%)	oil saturation (%)	porosity (<2 nm, %)	porosity (2−50 nm, %)	porosity (>50 nm, %)
G-1	3424.13	41.29	0.24	11.61	1.60	198.61	0.21	7.71	2.96	5.57	14.78	0.06	4.00	1.51
G-2	3426.25	44.04	0.22	18.72	1.40	184.80	0.18	7.71	1.60	4.42	13.21	0.05	3.07	1.30
G-3	3426.62	74.57	0.24	14.25	1.40	312.91	0.19	8.25	2.59	4.29	12.65	0.04	2.29	1.95
G-4	3429.50	55.37	0.21	16.33	1.22	202.69	0.18	9.46	1.84	5.07	9.35	0.06	3.33	1.68
G-5	3431.37	40.39	0.22	14.25	1.60	194.28	0.19	8.84	2.26	4.86	15.50	0.06	3.69	1.12
G-6	3433.12	41.62	0.22	17.49	1.50	186.98	0.19	7.20	2.41	5.47	13.41	0.06	4.13	1.28
G-7	3435.24	68.37	0.21	16.33	1.22	250.28	0.18	8.25	1.06	4.80	12.15	0.06	2.50	2.24
G-8	3437.36	56.87	0.24	11.61	1.84	313.56	0.24	11.61	1.84	4.34	23.21	0.04	2.48	1.82
G-9	3439.61	51.47	0.22	16.33	1.40	215.98	0.19	10.13	1.22	4.99	12.73	0.04	3.35	1.60
G-10	3441.23	22.76	0.24	10.84	1.50	102.25	0.21	8.25	2.59	5.24	15.27	0.04	4.71	0.49
G-11	3443.23	22.76	0.21	12.43	1.31	89.20	0.16	7.71	1.40	4.82	12.97	0.06	4.36	0.40
G-12	3445.23	44.24	0.21	22.98	0.99	131.95	0.17	8.84	1.14	6.44	10.12	0.06	5.18	1.19
G-13	3447.23	58.77	0.25	10.84	2.41	425.79	0.25	10.84	2.41	5.11	30.19	0.06	2.63	2.43
G-14	3449.23	48.37	0.24	17.49	1.50	217.31	0.21	7.71	2.96	5.66	17.21	0.06	3.83	1.77
G-15	3451.22	49.02	0.38	14.25	1.72	252.45	0.22	7.20	4.46	6.46	19.88	0.06	4.07	2.33
G-16	3453.10	49.62	0.25	10.13	3.17	472.37	0.27	8.84	3.17	5.07	36.09	0.06	2.85	2.16
G-17	3455.10	54.02	0.22	21.46	1.31	211.72	0.16	6.72	1.50	7.34	10.36	0.06	4.89	2.39
G-18	3456.47	46.17	0.24	17.49	1.50	207.42	0.19	7.20	3.40	5.88	15.59	0.05	4.01	1.82
G-19	3459.47	53.92	0.21	18.72	1.14	184.36	0.18	8.84	1.22	5.85	10.67	0.06	4.06	1.74
G-20	3461.09	61.17	0.21	17.49	1.14	209.14	0.19	7.71	1.60	6.28	11.80	0.05	3.95	2.28
G-21	3462.96	47.59	0.22	13.31	1.84	262.40	0.22	8.25	6.28	5.88	19.23	0.05	3.78	2.05
G-22	3465.21	27.41	0.27	10.84	2.26	185.48	0.24	3.64	2.77	5.71	23.62	0.70	4.45	0.56
G-23	3466.21	102.32	0.25	11.61	2.26	692.39	0.22	6.28	2.77	5.50	16.37	0.05	1.66	3.80
G-24	3467.08	40.01	0.22	13.31	1.50	179.75	0.19	11.61	4.46	6.53	12.58	0.05	4.81	1.67
G-25	3468.46	61.92	0.24	15.26	1.60	297.84	0.21	4.46	7.20	5.81	14.20	0.06	3.33	2.42
G-26	3470.08	61.42	0.22	16.33	1.40	257.73	0.18	7.20	1.72	6.14	10.39	0.05	3.63	2.45
G-27	3471.33	62.52	0.22	17.49	1.31	245.03	0.19	7.20	1.60	7.42	9.95	0.06	4.58	2.78
G-28	3472.83	49.62	0.24	11.61	1.60	238.67	0.21	6.28	2.59	6.23	12.97	0.06	4.11	2.06

sample no.	slope 1	D_1	R^2	slope 2	D_2	R^2	slope (>50 nm)	$D_{>50nm}$	R^2
G-1	1.57	1.4264	0.85	0.01	2.9931	0.74	0.01	2.9867	0.51
G-2	1.66	1.3433	0.84	0.01	2.992	0.81	0.01	2.9876	0.58
G-3	1.70	1.2984	0.83	0.00	2.9951	0.80	0.02	2.9796	0.35
G-4	1.75	1.2532	0.85	0.01	2.9925	0.77	0.02	2.984	0.45
G-5	1.74	1.2614	0.78	0.01	2.9937	0.74	0.01	2.9879	0.50
G-6	1.73	1.2673	0.78	0.00	2.996	0.69	0.01	2.9904	0.39
G-7	1.71	1.2915	0.85	0.01	2.9908	0.78	0.02	2.9785	0.45
G-8	1.61	1.3914	0.82	0.01	2.9949	0.71	0.02	2.9782	0.40
G-9	1.76	1.2398	0.80	0.01	2.9941	0.71	0.01	2.994	0.73
G-10	1.64	1.3622	0.83	0.00	2.9962	0.61	0.00	2.9951	0.62
G-11	1.64	1.3605	0.82	0.01	2.9915	0.73	0.01	2.991	0.77
G-12	1.85	1.1487	0.82	0.01	2.9949	0.76	0.01	2.9917	0.50
G-13	1.66	1.3436	0.75	0.01	2.994	0.56	0.03	2.9738	0.42

https://dx.doi.org/10.1021/acs.energyfuels.0c03978
Energy Fuels 2021, 35, 2209−2223

Table 1. continued

sample no.	slope 1	D_1	R^2	slope 2	D_2	R^2	slope (>50 nm)	$D_{>50nm}$	R^2
G-14	1.70	1.3041	0.84	0.00	2.9964	0.68	0.01	2.9872	0.34
G-15	1.68	1.3195	0.81	0.01	2.9913	0.70	0.02	2.9802	0.49
G-16	1.81	1.1912	0.69	0.01	2.993	0.58	0.03	2.9739	0.48
G-17	1.91	1.0875	0.74	0.00	2.9968	0.72	0.01	2.9882	0.32
G-18	2.13	0.8742	0.73	0.01	2.9938	0.74	0.02	2.985	0.44
G-19	1.80	1.2011	0.84	0.01	2.9946	0.73	0.01	2.988	0.42
G-20	1.73	1.2737	0.86	0.00	2.9973	0.71	0.01	2.9872	0.29
G-21	1.38	1.6173	0.85	0.01	2.9929	0.68	0.02	2.981	0.45
G-22	1.49	1.5108	0.82	0.01	2.9889	0.67	0.02	2.9835	0.69
G-23	1.44	1.5592	0.84	0.01	2.9884	0.68	0.05	2.952	0.45
G-24	1.60	1.3955	0.85	0.01	2.9937	0.74	0.01	2.9881	0.51
G-25	1.57	1.4332	0.85	0.01	2.9943	0.75	0.02	2.9807	0.38
G-26	1.64	1.364	0.85	0.01	2.9913	0.78	0.02	2.9798	0.46
G-27	1.76	1.2397	0.84	0.01	2.994	0.81	0.02	2.982	0.38
G-28	1.65	1.3466	0.83	0.01	2.9944	0.72	0.02	2.9848	0.41

using multiple regression based on Liu's laboratory data,[35] which were acquired from similar NMR experimental conditions to those of the present study. The relation could be expressed as

$$\rho = 0.65 \times X_q + 1.80 \times X_f - 10.78 \times X_p + 0.95 \times X_c + 3.82 \quad (6)$$

where ρ is the surface relaxivity (nm/ms) and X_q, X_f, X_p, and X_c are the contents of quartz, feldspar, pyrite and calcite (wt %), respectively. The fitting parameters are shown in Table 2. The significance F value of this regression is less than 0.001 with low error, supporting the reliability of this relation. Subsequently, the surface relaxivity of the MES shales could be calculated according to the previous study[9] (Table 1). The surface relaxivities of the MES shales range from 22.76 to 102.32 μm/s with an average value of 51.34 μm/s, which corresponds to the proposed 30−300 μm/s for clastics.[17] Due to the water-wetting properties of the MES shales, the calculated surface relaxivity is only appropriate for brine-saturated samples. Here, the pore size distribution of the brine-saturated MES shale samples could be obtained as shown in Figure 6c. The dominant pore space size ranges from 2 to 260.53 nm, followed by a pore space size ranging from 0.75 to 3.95 μm. This pore size distribution means that the immovable fluid principally occurs in the nanoscale pore space and that the movable fluid is mainly distributed in the micrometer-sized pore space.

5.4. Porosity and Oil Saturation. As indicated in Table 1, the bulk porosities of the MES shales range from 4.29 to 7.41% with an average of 5.61%. The oil saturation ranges from 9.35−36.09%, with a mean of 15.59%, which is higher than that in the Dongying Sag with an oil saturation of 1−8%.[51] The pores could be divided into micropores (<2 nm), mesopores (2−50 nm), and macropores (>50 nm).[52] According to the calculated pore size distribution, the proportions of these three pore types can be obtained, as shown in Figure 8. The pore space is dominated by mesopores ranging, 30.19−90.43% (avg 65.88%), followed by macropores (2.26−68.97%, avg 32.74%). The micropores occupy the lowest percentage, 0.71−12.22% (avg 1.38%).

5.5. Fractal Characteristic. The T_2 relaxation reveals a complex pore structure in the MES shales. Furthermore, because the self-similarity requirement is satisfied for the geometry of complex rock pores, the degree of irregularity of the pore geometry could be quantitatively described by using fractal analysis with the fractal dimension.[53−55] On the basis of the NMR T_2 relaxation, the fractal dimension could be calculated by[56]

$$\lg(V) = (3 - D)\lg(T_2) + (D - 3)\lg(T_{2max}) \quad (7)$$

where V is the cumulative pore volume fraction. The fractal dimension (D) of pore space ranges from 2 to 3, and higher D values indicate a more complex and heterogenic pore space.[55] D could be obtained from the slope of the plot of lg(V) versus lg(T_2) for each sample. For the brine-saturated samples, the fractal dimensions from NMR could quantify the complexity and heterogeneity of the pore structure. All the MES shale samples show two distinct segments in the plots of lg(V) versus lg(T_2) with a demarcation point of T_0, which corresponds perfectly to the boundary of immovable and movable fluid pore spaces (Figure 6c). Therefore, the complexity of the immovable and movable fluid pore spaces could be quantified by using the fractal dimensions D_1 and D_2,

https://dx.doi.org/10.1021/acs.energyfuels.0c03978
Energy Fuels 2021, 35, 2209−2223

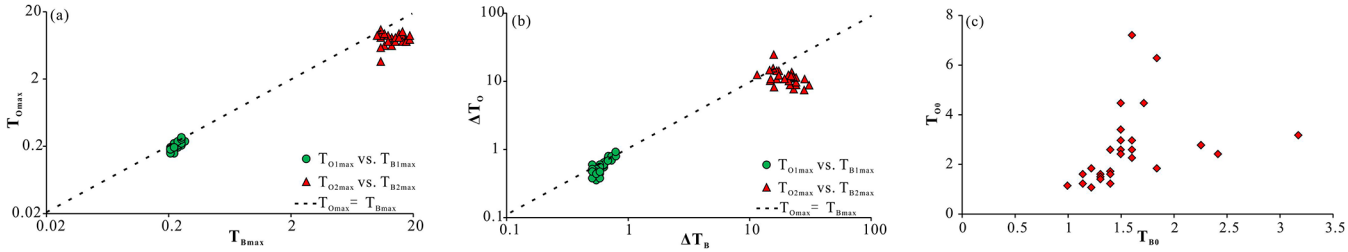

Figure 7. Plots of NMR T_2 distribution parameters used in this study for MES shale samples. (a) Relative positions of brine and oil T_2 distribution. T_{Omax} and T_{Bmax} are the T_2 relaxation times at peaks of brine and oil T_2 distributions, respectively. (b) Breadths of brine and oil T_2 distributions. ΔT_O and ΔT_B are the difference values of T_2 relaxation times at half of peaks of brine and oil T_2 distributions respectively. (c) Disordered correlation between T_{B0} and T_{O0} values, which are the end T_2 relaxation time of the first wave of brine and oil T_2 distributions, respectively.

Table 2. Summary Output of Multiple Regression

variables	coefficients	standard error	*t* stat	*p*-value	lower 95%	upper 95%
intercept	3.82	1.12	3.41	0.08	−1.00	8.64
X_q	0.65	0.03	24.16	0.00	0.54	0.77
X_f	1.80	0.09	20.86	0.00	1.43	2.17
X_p	−10.78	0.25	−43.71	0.00	−11.84	−9.72
X_c	0.95	0.04	25.71	0.00	0.79	1.11
variance analysis						
regression	SS: 538.86	MS: 134.71		*F*: 1529.50	significance $F < 0.001$	
residual	SS: 0.18	MS: 0.09				
regression statistics						
R^2: 0.99				standard error: 0.30		

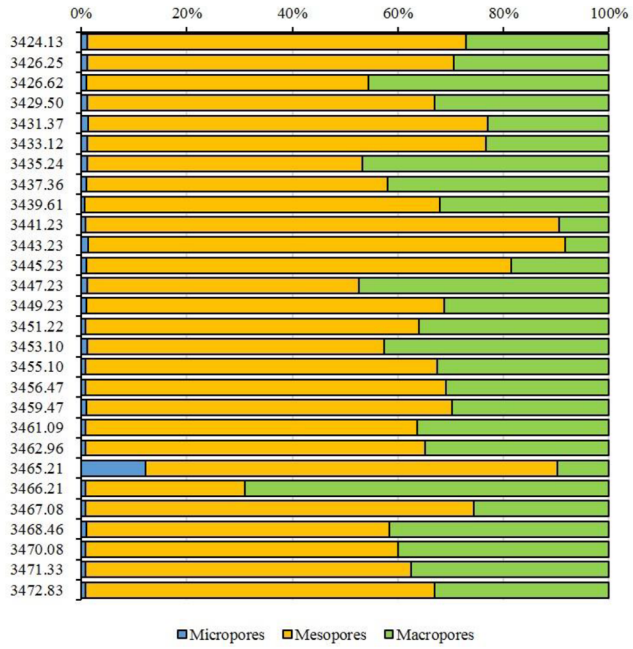

Figure 8. Percentage variations of micropores, mesopores, and macropores in MES shales.

respectively. For the MES shales, the D_1 values range from 1.0875 to 1.6173 except for an anomalous low value of 0.8742 in sample G-27, while the D_2 value ranges from 2.9844 to 2.9973 (Table 1). Due to the D values ranging from 2 to 3, all D_1 values are less than 2; thus the result is invalid.[55]

The fractal study on the tight sand reservoir also showed the low dimensionality (<2) of the immovable pore space by using NMR.[56] This phenomenon may be caused by the use of the incorrect model for calculating the fractal dimension of immovable pore space using NMR. Equation 7 in Shao's study is obtained calculated based on the spherical model.[56] This equation assumes that the pores in the reservoir exhibit isolated spherality. Apparently, the immovable pore cannot be regarded as isolated sphere according the calculated low D_1 values in the studies of shale and sandstone. In reality, pores in reservoirs are complex and include vast platelike, tubulose, and other irregular shapes[55] (Figure 4). The low dimensions in immovable pore systems indicate that the spherical model is not appropriate for calculating the dimensionality of a complex immovable pore space.

All D_2 values are close to 3, indicating a more complex pore system and self-similarity for the movable pore space. This phenomenon may be caused by the pore throats, which represent an important factor controlling the fractal dimension and promote fluid flow.[55] For isolated pores, the fractal dimension is not closely related to their size due to their self-similarity. However, throats connect the isolated pores and make the pore structure more complex, which leads to a higher D value. For large pore spaces, the r_0 and P_{B2max} values have clear negative correlations with the D_2 value (Figure 9a,b). Thus, the more complex pore structure system will lead to a lower pore size boundary for fluid flow and a decreased fluidal space, which may be influenced by the existence of throats to a great extent. Furthermore, the fractal dimensions of the macropores ($D_{>50nm}$) were also calculated as listed in Table 1, and the $D_{>50nm}$ value is generally lower than the D_2 value. This finding implies that the movable pore space is more complex, further supporting that the throats in a porous medium enhance its complexity and heterogeneity but promote liquid flow.

https://dx.doi.org/10.1021/acs.energyfuels.0c03978
Energy Fuels 2021, 35, 2209−2223

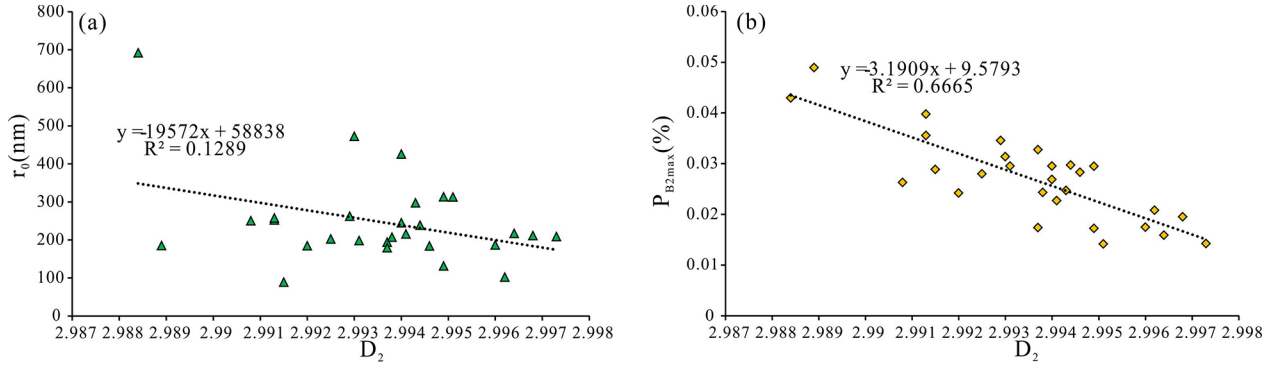

Figure 9. Plots of r_0 vs D_2 (a) and P_{B2max} vs D_2 (b) show two negative correlations of fractal dimension (D_2) with the pore size boundary of immovable and movable fluids (r_0) as well as a relatively larger pore space.

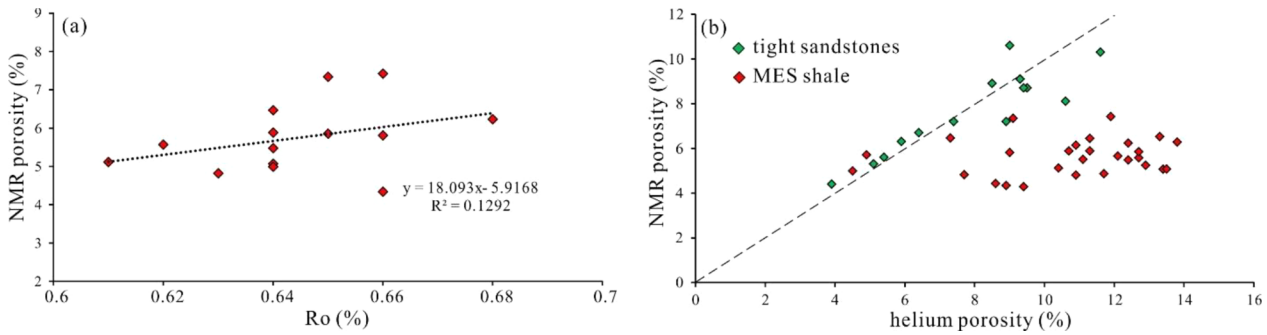

Figure 10. Positive relation between NMR porosity and R_o (a), which indicates that high thermal maturity promotes the development of pore space in MES shales. (b) Difference in NMR and helium porosity measurements in tight sandstones and shale sediments. The tight sandstone porosities are cited from Shao et al.[56]

6. DISCUSSION

6.1. Factors Affecting Shale Porosity. The pore structure of the MES shales is slightly different from that of the lacustrine Chang-7 shales in the Ordos Basin in terms of their micropore and macropore portions.[57] For the Chang-7 shales, the mesopores contribute most of the pore space, and the contributions of the micro- and macropores are low. In addition, a large percentage of the pore space is attributed to pore sizes larger than 10 μm for the Chang-7 shales, which is rarely observed in the MES shales. Three factors may lead to these differences, including the thermal maturity, the T_2 relaxation mechanism, and sample preparation. The thermal maturity of the MES shales is relatively low, with a thermal maturity (R_o) less than 0.7%, which is lower than that of the Chang-7 shales in the Ordos Basin, which have a R_o of 0.91%. The low thermal maturity would lead to undeveloped organic nanopores, as shown in the SEM observation (Figure 4). In contrast, a higher maturity would facilitate nanopore development in shales sediments, as supported by the positive correlation between bulk porosity and R_o (Figure 10a). Moreover, the pore structure was obtained by using the T_2 surface relaxation mechanism. The hydrocarbon in smaller nanopore space approaches that of dead oil in low maturity shales, and the viscosity is high due to the low maturity. Therefore, the relaxation mechanism in the smaller pores maybe dominated by bulk relaxation.[17] In addition, the liquid invasion methods used in the previous study by Jiang et al.[57] would break the pore structure by producing cracks, which would result in errors in the estimates of macropore proportions. In contract, the NMR technique is non-destructive, and the macropore proportions detected are relatively reliable.[17,30]

The NMR porosity in this study is obviously lower than that measured by using the helium method employed by Chen et al.[9] However, the NMR porosity is close to the helium porosity for tight sandstones[56] (Figure 10b). This phenomenon reveals the important influence of lithology on the NMR porosity measurements. For shale sediments, clay minerals occupy a dominant portion, with an average content of 42.75% in the MES shales.[9] The high clay content would cause serious swelling when the samples encounter water.[58] In addition, the brine concentration is 3%, which is lower than that in Shao et al.'s study. These factors may lead to the low porosity and low portion of nanopores.

6.2. Oil Relaxation Mechanisms in the MES Shales. For the oil in low-maturity EMS shales, the drilling tested viscosity is high, approaching 11.03 cP (50 °C) as drilling tested at 3422.6−3436.2m, which is considerably higher than the values reported by Zhao et al.[59] Therefore, the oil T_2 distributions should be explained by the bulk relaxation in this study. In this study, NMR experiments were performed at 308.15 K (35 °C); therefore, the relationship between the oil T_2 relaxation time and viscosity can be described as

$$T_{2\text{bulk}} = 2.20 \times \frac{1}{\eta} \tag{8}$$

Hence, the oil T_2 relaxation time could reflect the volume proportions of the liquids with different viscosities. For the MES shales, the dominant oil viscosity ranges from 2 to 70 cP, followed by 0.1−0.7 cP (Figure 6d). The drilling tested oil viscosity of 11.03 cP occupies a large proportion (Figure 6d),

https://dx.doi.org/10.1021/acs.energyfuels.0c03978
Energy Fuels 2021, 35, 2209−2223

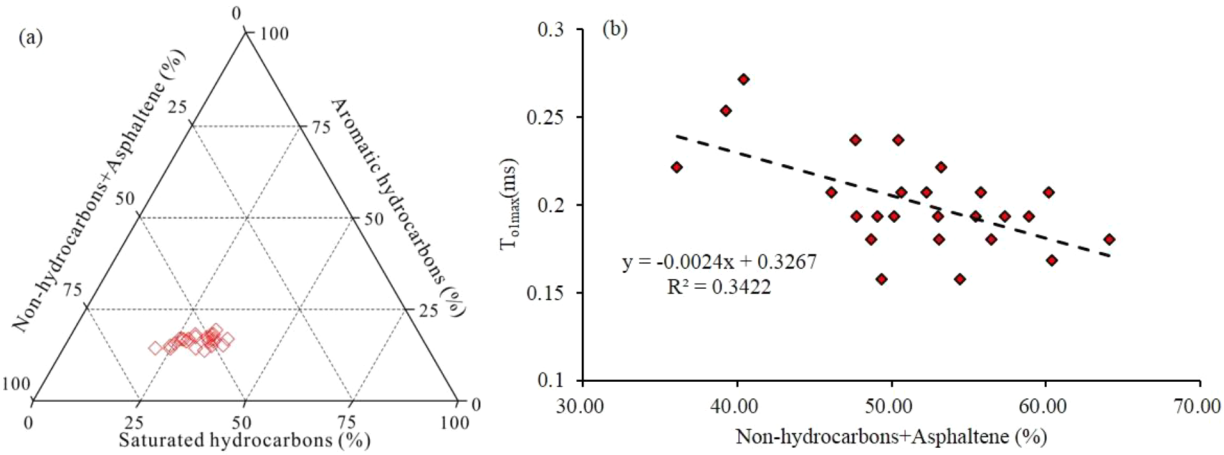

Figure 11. Ternary diagram of extracted components of MES shales (a) and negative relation between T_{1omax} and nonhydrocarbons and asphaltene (b).

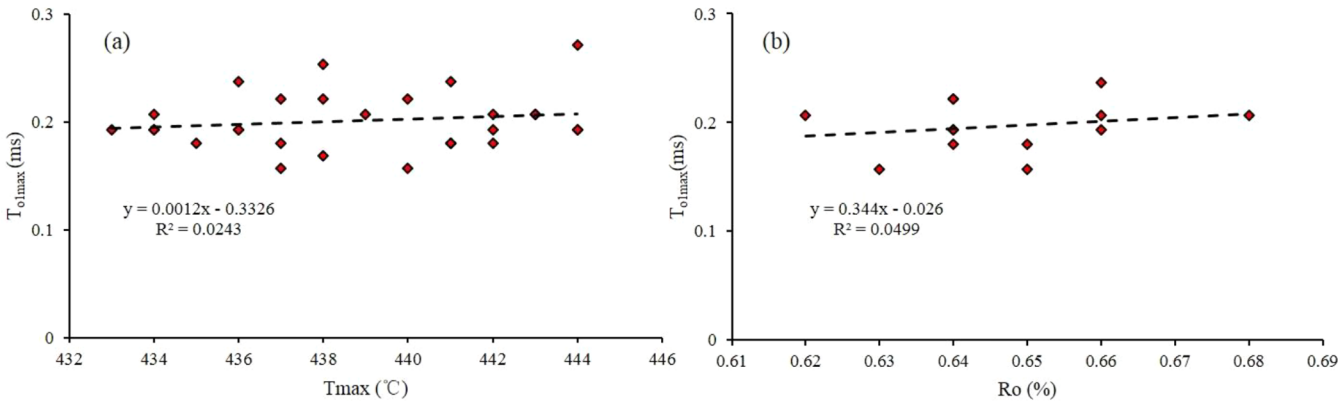

Figure 12. Positive correlations of T_{O1max} with T_{max} and R_o show that high oil viscosity is correlated with low thermal maturity.

which further powerfully supports the bulk relaxation explanation. The extracted components show that the residual oil in the MES shales has high non-hydrocarbon and asphaltene contents with the mean sum value of 51.61% (Figure 11a). The high resin content mainly relates to the low thermal maturity[60] and leads to viscous oil. In addition, the T_{O1max} values have an obvious negative correlation with non-hydrocarbon and asphaltene contents (Figure 11b), which cross-check the viscosity interpretation by using bulk relaxation. Furthermore, the oil viscosity of the MES shale oil is relatively lower than that in the Dongying Sag, ranging from approximately 0.8−200 cP[21] (Figure 6f). In addition, the temperature of NMR experiments is 35 °C, while the temperature and pressure underground are higher. The actual viscosity underground would be lower than the explained viscosity in this study. This difference implies the good shale oil potential and oil mobility for the MES shales.

6.3. Oil Mobility in the MES Shales. It is not necessary to discuss mobility for gas, but mobility is an important consideration for oil, especially in shale sediments. The pore structure and liquid properties are two important aspects that should be considered in the study of the mobility of liquids in shale sediments. On the one hand, the position of the liquid peaks in the T_2 distribution could reflect oil properties.[17] Heavy oil with a high viscosity would have a shorter T_2 relaxation time compared to a light oil with a low viscosity, because the viscosity will greatly affect the polar molecule relaxation behavior in a magnetic field.[17] Therefore, oil typing can be easy in water-wet rocks according to the moderate peak width and distinct position in the T_2 distribution. For the water-wet MES shales, the generally lower T_{Omax} values imply the relatively higher oil viscosity in the MES shales.[17] The T_{O1max} value is positively correlated with R_o and T_{max} values (Figure 12), which implies that the high-viscosity oil may be associated with its low thermal maturity.[60] The characteristics of the shale oil in the Dongying Sag shows that the shale oil could attain an acceptable productivity when the viscosity is lower than 10 cP[21] (Figure 6f). The oil with viscosity lower than 10 cP is in the range of 43.33−65.12% (avg 53.66%) of the total oil-filling pore space in the MES shales. There may be higher proportion of mobility underground due to the high temperature and pressure underground. These features indicate good mobility in the MES shales.

On the other hand, the pore structure information could also be obtained from the brine-saturated T_2 distribution. An interesting phenomenon was observed in this study: The pores corresponding to T_{B0} are larger than 50 nm, which means that all brine water in the micro- and mesopores as well as in some macropores is immovable in the MES shale samples. Because the brine viscosity (0.2−0.8 cP) is notably lower than that of oil (0.2−1000 cP), the high-viscosity oil cannot move in the pore spaces where brine is immovable.[17] Therefore, only parts macropores of the MES shales are available for oil flow. According to the percentages of the micro-, meso-, and

https://dx.doi.org/10.1021/acs.energyfuels.0c03978
Energy Fuels 2021, 35, 2209−2223

Table 3. Comparison of Geological Conditions for Shale Oil-Producing Areas[a]

basins/ depressions	layers	TOC (%)	R_o (%)	porosity (%)	thickness (m)	yields	density (g/cm^3)	pressure coefficient
Songliao	Qinshankou	2.0−3.0	0.5−1.3	1.4−8.7	40−150	1−10.23 (m^3/d)	0.82−0.85	1.0−1.2
Jiyang	Shahejie	3.0−10.0	0.5−1.3	2.0−12.4	100−250	2−110 (t/d)	0.67−0.86	1.2−1.9
Nanxiang	Hetaoyuan	0.78−7.64	0.58−0.74	3.2−7.29	200−600	4.68−28.1 (m^3/d)	0.82−0.90	1.2−1.3
Jianghan	Qianjiang	1.0−10.0	0.41−0.76	1.0−13.0	10−50	1.4−10000 (t/d)	0.80−1.05	0.87−2.05
Ordos	Yanchang	5.0−16.0	0.6−1.1	2.0−12.0	30−70	−23.85 (m^3/d)	0.80−0.85	0.7−0.9
Qaidam	Shimengou	0.6−10.7	0.36−0.66	3.0−10.3	∼30	0.5−4 (t/d)	N.A.	1.3−1.4
Subei	Funing	0.5−5.0	0.5−1.3	0.2−6.8	50−500	2−36.83 (t/d)	0.81−0.85	1.0−1.1
Junggar	Lucaogou	3.0−12.0	0.6−1.2	5.45−8.35	100−240	17.9 (t/d)	0.87−0.92	1.2−1.5
Santanghu	Lucaogou	1.0−6.0	0.6−1.1	2.0−12.0	10−100	0.01−22.2 (m^3/d)	0.85−0.9	1.0−1.2
Alberta	Cardium	<2.5	>0.7	N.A.	50−150	20−70 (t/d)	0.82−0.85	>1.3
Williston	Bakken	3.0−25.0	0.6−0.9	5−13.0	5−49	210 (t/d)	0.81−0.83	1.2−1.5
Permian	Wolfcamp/Spraberry	2.2−7.2	0.7−1.7	4−12.0	20−150	80 (t/d)	0.78−0.84	1.0−1.4
Gulf	Eagle Ford	3.0−7.0	0.7−1.4	2−12.0	20−60	200(t/d)	0.82−0.87	1.3−1.8
Denver	Niobrara	1.0−6.0	0.67−0.95	N.A.	200−450	20.7 (m^3/d)	0.825	N.A.
Neuken	Vaca Muerta	3.0−5.0	0.7−1.3	N.A.	40−150	24.3−81 (t/d)	0.80−0.83	1.5−2.3
Cangdong Sag	Ek_2	0.3−12.9	0.45−0.84	1−9.0	200−800	29.6 (t/d)	0.87−0.91	1.16−1.18
Nanpu sag	EMS shales	0.81−6.61	0.62−0.68	4.3−7.4	198.5	N.A.	0.85−0.88	1.24−1.41

[a]The data are from Wang et al.[67] and Zhao et al.[68]

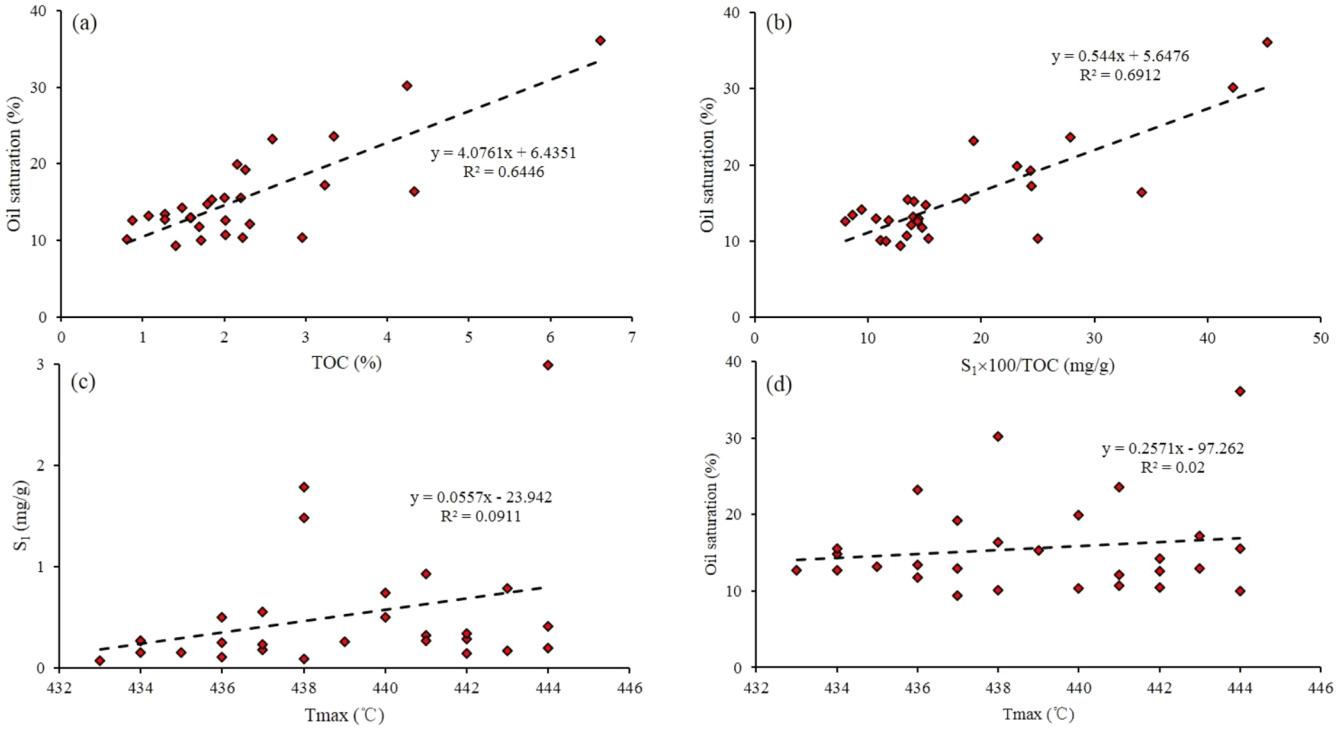

Figure 13. Oil saturation shows positive correlations with TOC content (a) and $S_1 \times 100$/TOC (b) for the MES shales in the Nanpu Sag. (c) and (d) Free hydrocarbon (c) and oil saturation (d) have positive relations with thermal maturity.

macropores in Figure 8, the movable oil in the MES shales does not exceed the macropore percentage of 2.26−68.97% (avg 32.74%).

6.4. Shale Oil Potential. Compared to the main shale oil-producing areas (Table 3), the geological conditions of MES shales are similar to those of Eocene Hetaoyuan and Ek_2 shale sediments. The maturity of shale oil reservoirs in China is commonly lower than those overseas. Due to the relatively low maturity, the oil density in MES shales is relatively high, which is similar to those in Qiangjiang shales, Ek_2 shales, Hetaoyuan shales, and Lucagou shales. All of the shale oil reservoirs are characterized by overpressure except the Yanchang shales. The pressure coefficient in MES shales is 1.24−1.41, which is relatively high compared to other shale sediments and provides good conditions for oil flow. Therefore, MES shales have similar or better geological conditions than those found in other shale oil-producing areas. In addition, the oil saturation has notable positive correlations with TOC contents as well as with the ratio of $S_1 \times 100$/TOC, as shown in Figure 13a,b. Previous studies suggest that good shale oil potential is accompanied by an $S_1 \times 100$/TOC ratio higher than 100.[3,8,61] On the basis of the positive relationship in this study (Figure 13b), this threshold value corresponds to the oil saturation of approximately 60.05% for the MES shales. In general, sand

https://dx.doi.org/10.1021/acs.energyfuels.0c03978
Energy Fuels 2021, 35, 2209−2223

reservoirs with an oil saturation higher than 40% are regarded as good hydrocarbon-bearing reservoirs. Therefore, the previous threshold is unduly restrictive and unreasonable for the evaluation of the shale oil potential in low-maturity lacustrine shales. Moreover, the positive relationships of S_1 value and oil saturation with thermal maturity (Figure 13c,d) imply high shale potential at a deeper position.

Comprehensive analysis shows that the shale oil potential in the MES shales at Nanpu Sag is very promising, as evidenced by six points: (1) The relation of oil saturation and S_1 value suggests that the evaluation threshold of shale oil potential may be unduly restrictive for the low-maturity lacustrine shale sediments. (2) The brittle MES shales have good condition for horizontal well fracturing, which will immensely improve pore structure. (3) The low-viscosity oil (<10 cP) in the MES shales occupies a considerable proportion under lab conditions, which is beneficial for oil flow in the MES shales. (4) The low-maturity MES shales could be heated underground by using the development of in situ conversion process technology,[62−65] which could fortify the hydrocarbon potential and reduce the viscosity to facilitate hydrocarbon flow. (5) The geological conditions of MES shales are similar to those of other shales oil-producing areas. (6) The sampling well is located at a relatively high tectonic position due to ocean constraints; therefore, the MES shales at deeper positions may have good shale oil potential.

7. CONCLUSIONS

On the basis of NMR experiments, the pore structure of the low-maturity MES shales was analyzed, and the oil properties and mobility as well as shale oil potential were further evaluated in this study. The pore space in the low-maturity MES shales spans the range of nano- to microscale with various pore types and is dominated by mesopores. The NMR porosity of the MES shale ranges from 4.29 to 7.41%, with oil saturation in the range of 9.35−36.09%. The pore space for fluid flow is complex and has good self-similarity with high fractal dimensions, while this portion occupies less than 32.74% of total pore space in the MES shales. The abundance of brittle minerals with relatively a high brittleness index indicate that the MES shales have good brittleness, which is advantageous for fracturing in the process of shale oil exploration. Considering the high viscosity and the dead oil, the NMR relaxation mechanism in nanoporous low-maturity shales is proposed according to bulk relaxation. The oil viscosity of MES shale ranges from 2 to 70 cP. The movable oil with viscosity lower than 10 cP accounts for 53.66% of the total oil-filling pore space. For the MES shales, thermal maturity has influence on the porosity, viscosity, free hydrocarbon content, and oil saturation in the rocks. Higher thermal maturity would facilitate the affected pore space development with higher porosity, enhance the free hydrocarbon content and oil saturation, and reduce the oil viscosity to some extent. The MES shales have geological conditions similar to those of other shale oil-producing areas. These findings indicate the suitable and promising shale oil potential of the brittle MES shales at low tectonic positions in the Nanpu Sag when accompanied by the technologies of in situ conversion process and hydraulic fracturing. This study also provides a new consideration of the NMR in shale sediments, especially for low-maturity shales. When discussing the oil in nanopores, the bulk relaxation mechanism needs to be considered. In the future research, the relaxivity and isolated pore should be taken into account in the study of low-maturity shale sediments by using NMR technology.

AUTHOR INFORMATION

Corresponding Authors

Xiongqi Pang − *State Key Laboratory of Petroleum Resources and Prospecting, China University of Petroleum, Beijing 102249, China*; Email: pangxqcup@163.com

Fujie Jiang − *State Key Laboratory of Petroleum Resources and Prospecting, China University of Petroleum, Beijing 102249, China*; orcid.org/0000-0002-0089-2972; Email: jfjhtb@163.com

Authors

Di Chen − *State Key Laboratory of Petroleum Resources and Prospecting, China University of Petroleum, Beijing 102249, China*

Guoyong Liu − *PetroChina Jidong Oilfield Company, Tangshan 063004, China*

Zhihong Pan − *Department of Physics, University of Alberta, Edmonton, Alberta T6G 2E1, Canada*

Yang Liu − *State Key Laboratory of Petroleum Resources and Prospecting, China University of Petroleum, Beijing 102249, China*

Complete contact information is available at: https://pubs.acs.org/10.1021/acs.energyfuels.0c03978

Notes

The authors declare no competing financial interest.

ACKNOWLEDGMENTS

This study was supported by the National Science and Technology Major Project of the Ministry of Science and Technology of China (2016ZX05006-006-001) and AAPG Foundation Grants-in-Aid program (14545976 and 13231). We express our gratitude to Jidong Oilfield, China National Petroleum Corporation (CNPC), for providing basic geological data. We thank the experts Xiao Liu and Lingjian Meng at the research institute of Jidong Oilfield for their help in this study. We are also grateful to the people who provided helpful comments and assisted in the process of writing this manuscript.

REFERENCES

(1) Ambrose, R. J.; Hartman, R. C.; Diaz Campos, M.; Akkutlu, L. Y.; Sondergeld, C. New pore-scale considerations for shale gas in place calculations. *SPE Unconventional Gas Conf.* **2010**, 131772-MS.

(2) Clarkson, C. R.; Jensen, J. L.; Pedersen, P. K.; Freeman, M. Innovative methods for flow unit and pore-structure analyses in a tight siltstone and shale gas reservoir. *AAPG Bull.* **2012**, *96* (2), 355−374.

(3) Jarvie, D. M. Shale resource systems for oil and gas: Part 2 shale-oil resource systems. *AAPG Memoir* **2012**, *97*, 89−119.

(4) Mastalerz, M.; Schimmelmann, A.; Drobniak, A.; Chen, Y. Porosity of Devonian and Mississippian New Albany Shale across a maturation gradient: Insights from organic petrology, gas adsorption, and mercury intrusion. *AAPG Bull.* **2013**, *97* (10), 1621−1643.

(5) Akkutlu, I. Y.; Baek, S.; Olorode, O. M.; Wei, P.; Zhang, T.; Shuang, A. Shale Resource Assessment in Presence of Nanopore Confinement. *URTeC 2017* **2017**, 2670808-MS.

(6) Li, M.; Chen, Z.; Ma, X.; Cao, T.; Qian, M.; Jiang, Q.; Tao, G.; Li, Z.; Song, G. Shale oil resource potential and oil mobility characteristics of the Eocene-Oligocene Shahejie Formation, Jiyang Super-Depression, Bohai Bay Basin of China. *Int. J. Coal Geol.* **2019**, *204*, 130−143.

(7) Jiang, F.; Pang, X.; Bai, J.; Zhou, X.; Li, J.; Guo, Y. Comprehensive assessment of source rocks in the Bohai Sea area, eastern China. *AAPG Bull.* **2016**, *100* (6), 969−1002.
(8) Li, M.; Chen, Z.; Cao, T.; Ma, X.; Liu, X.; Li, Z.; Jiang, Q.; Wu, S. Expelled oils and their impacts on rock-eval data interpretation, Eocene Qianjiang Formation in Jianghan Basin, China. *Int. J. Coal Geol.* **2018**, *191*, 37−48.
(9) Chen, D.; Pang, X.; Wang, Y.; Dong, T.; Jiang, F.; Li, L.; Pang, H.; Bai, H.; Pang, B.; Qin, R.; Jiang, H. Palaeoenvironmental periodisms of middle Eocene terrestrial sediments in Bohai Bay Basin, eastern China, and their implications for organic matter accumulation. *Mar. Pet. Geol.* **2020**, *112*, 104060.
(10) Xie, X.; Krooss, B. M.; Littke, R.; Amann-Hildenbrand, A.; Li, M.; Li, Z.; Snowdon, L. R.; Mohnhoff, D. Accessibility and mobility of hydrocarbons in lacustrine shale: Solvent flow-through extraction experiments on Eocene oil shales from Bohai Bay Basin, eastern China. *Org. Geochem.* **2019**, *127*, 23−36.
(11) Ross, D. J. K.; Bustin, R. M. The importance of shale composition and pore structure upon gas storage potential of shale gas reservoirs. *Mar. Pet. Geol.* **2009**, *26* (6), 916−927.
(12) Bustin, R. M.; Bustin, A. M. M.; Cui, A.; Ross, D.; Pathi, V. M. Impact of shale properties on pore structure and storage characteristics. *SPE Shale Gas Production Conf.* **2008**, 119892.
(13) Li, M.; Chen, Z.; Qian, M.; Ma, X.; Jiang, Q.; Li, Z.; Tao, G.; Wu, S. What are in pyrolysis S_1 peak and what are missed? Petroleum compositional characteristics revealed from programed pyrolysis and implications for shale oil mobility and resource potential. *Int. J. Coal Geol.* **2020**, *217*, 103321.
(14) Chalmers, G. R. L.; Bustin, R. M.; Power, I. M. Characterization of gas shale pore systems by porosimetry, pycnometry, surface area, and field emission scanning electron microscopy transmission electron microscopy image analyses: examples from the Barnett, Woodford, Haynesville, Marcellus, and Doig units. *AAPG Bull.* **2012**, *96*, 1099−1119.
(15) Clarkson, C. R.; Solano, N.; Bustin, R. M.; Bustin, A. M. M.; Chalmers, G. R. L.; He, L.; Melnichenko, Y. B.; Radliński, A. P.; Blach, T. P. Pore structure characterization of North American shale gas reservoirs using USANS/SANS, gas adsorption, and mercury intrusion. *Fuel* **2013**, *103*, 606−616.
(16) Straley, C.; Rossini, D.; Vinegar, H. J.; Tutunjian, P.; Morriss, C. Core analysis by low-field NMR. *The Log Analyst* **1997**, *38*, 84−93.
(17) Coates, G. R.; Xiao, L.; Prammer, M. G. *NMR Logging: Principles and Applications*; Haliburton Energy Services, Houston, TX, 1999.
(18) Yao, Y.; Liu, D.; Che, Y.; Tang, D.; Tang, S.; Huang, W. Petrophysical characterization of coals by low-field nuclear magnetic resonance (NMR). *Fuel* **2010**, *89* (7), 1371−1380.
(19) Firouzi, M.; Rupp, E. C.; Liu, C. W.; Wilcox, J. Molecular simulation and experimental characterization of the nanoporous structures of coal and gas shale. *Int. J. Coal Geol.* **2014**, *121*, 123−128.
(20) Zolfaghari, A.; Dehghanpour, H.; Xu, M. Water sorption behaviour of gas shales: II Pore size distribution. *Int. J. Coal Geol.* **2017**, *179*, 187−195.
(21) Chen, W. Research on the Movability of Shale Oil in Dongying Sag and the Optimization Method of Favorable Zone. Master degree thesis, China University of Petroleum, 2017.
(22) Li, W.; Pang, X.; Snape, C.; Zhang, B.; Zheng, D.; Zhang, X. Molecular Simulation Study on Methane Adsorption Capacity and Mechanism in Clay Minerals: Effect of Clay Type, Pressure, and Water Saturation in Shales. *Energy Fuels* **2019**, *33* (2), 765−778.
(23) Mosher, K.; He, J.; Liu, Y.; Rupp, E.; Wilcox, J. Molecular simulation of methane adsorption in micro-and mesoporous carbons with applications to coal and gas shale systems. *Int. J. Coal Geol.* **2013**, *109−110*, 36−44.
(24) Collell, J.; Galliero, G.; Gouth, F.; Montel, F.; Pujol, M.; Ungerer, P.; Yiannourakou, M. Molecular simulation and modelisation of methane/ethane mixtures adsorption onto a microporous molecular model of kerogen under typical reservoir conditions. *Microporous Mesoporous Mater.* **2014**, *197*, 194−203.
(25) Sharma, A.; Namsani, S.; Singh, J. K. Molecular simulation of shale gas adsorption and diffusion in inorganic nanopores. *Mol. Simul.* **2015**, *41*, 414−422.
(26) Ross, D. J. K.; Bustin, R. M. Characterizing the shale gas resource potential of Devonian Mississippian strata in the western Canada sedimentary basin: application of an integrated formation evaluation. *AAPG Bull.* **2008**, *92* (1), 87−125.
(27) Chalmers, G. R. L.; Ross, D. J. K.; Bustin, R. M. Geological controls on matrix permeability of Devonian gas shales in the Horn River and liard basins, northeastern british Columbia, Can. *Int. J. Coal Geol.* **2012**, *103*, 120−131.
(28) Hou, H.; Shao, L.; Li, Y.; Lu, J.; Li, Z.; Wang, S.; Zhang, W.; Wen, H. Geochemistry, reservoir characterization and hydrocarbon generation potential of lacustrine shales: A case of YQ-1 well in the Yuqia Coalfield, northern Qaidam Basin, NW China. *Mar. Pet. Geol.* **2017**, *88*, 458−471.
(29) Al-Mahrooqi, S. H.; Grattoni, C. A.; Moss, A. K.; Jing, X. An investigation of the effect of wettability on NMR characteristics of sandstone rock and fluid systems. *J. Pet. Sci. Eng.* **2003**, *39* (3−4), 389−398.
(30) Hodgkins, M. A.; Howard, J. J. Application of NMR Logging to Reservoir Characterization of Low-Resistivity Sands in the Gulf of Mexico. *AAPG Bull.* **1999**, *83* (1), 114−127.
(31) Cohaut, N.; Blanche, C.; Dumas, D.; Guet, J. M.; Rouzaud, J. N. A small angle X-ray scattering study on the porosity of anthracites. *Carbon* **2000**, *38*, 1391−400.
(32) Hassan, J. Pore size distribution calculation from 1H NMR signal and N_2 adsorption-desorption techniques. *Phys. B* **2012**, *407* (18), 3797−3801.
(33) Yao, Y.; Liu, D. Comparison of low-field NMR and mercury intrusion porosimetry in characterizing pore size distributions of coals. *Fuel* **2012**, *95*, 152−158.
(34) Hinai, A.; Rezaee, R.; Esteban, L.; Labani, M. Comparisons of pore size distribution: a case from the Western Australian gas shale formations. *Journal of Unconventional Oil and Gas Resources* **2014**, *8*, 1−13.
(35) Liu, Y.; Yao, Y.; Liu, D.; Zheng, S.; Sun, G.; Chang, Y. Shale pore size classification: An NMR fluid typing method. *Mar. Pet. Geol.* **2018**, *96*, 591−601.
(36) Allen, M. B.; Macdonald, D. I. M.; Xun, Z.; Vincent, S. J.; Brouet-Menzies, C. Early Cenozoic two-phase extension and late Cenozoic thermal subsidence and inversion of the Bohai Basin, northern China. *Mar. Pet. Geol.* **1997**, *14* (7−8), 951−972.
(37) Dong, Y.; Xiao, L.; Zhou, H.; Wang, C.; Zheng, J.; Zhang, N.; Xia, W.; Ma, Q.; Du, J.; Zhao, Z.; Huang, H. The Tertiary evolution of the prolific Nanpu Sag of Bohai Bay Basin, China: Constraints from volcanic records and tectono-stratigraphic sequences. *Geol. Soc. Am. Bull.* **2010**, *122* (3−4), 609−626.
(38) Zou, Y. R.; Sun, J. N.; Li, Z.; Xu, X.; Li, M.; Peng, P. Evaluating shale oil in the Dongying Depression, Bohai Bay Basin, China, using the oversaturation zone method. *J. Pet. Sci. Eng.* **2018**, *161*, 291−301.
(39) Pu, X. Major Oil Discovery Made in China's Bohai Bay Basin, *AAPG Explorer*, 2019. https://explorer.aapg.org/story/articleid/52149/major-oil-discovery-made-in-chinas-bohai-bay-basin.
(40) Bao, Y.; Zhang, L.; Zhang, J.; Li, J.; Li, Z. Factors influencing mobility of Paleogene shale oil in Dongying Sag, Bohai Bay Basin. *Oil Gas Geol.* **2016**, *37* (3), 408−414.
(41) Liang, C.; Cao, Y.; Jiang, Z.; Wu, J.; Guoqi, S.; Wang, Y. Shale oil potential of lacustrine black shale in the Eocene Dongying depression: Implications for geochemistry and reservoir characteristics. *AAPG Bull.* **2017**, *101*, 1835−1858.
(42) Zheng, H. J.; Dong, Y. X.; Zhu, G. Y.; Wang, X. D.; Xiong, Y. High-quality source rocks in Nanpu Sag. *Petrol. Explor. Dev.* **2007**, *34* (4), 385−391.
(43) Freeman, J. J.; Hofman, J. P.; Appel, M.; Perkins, R. B. Restricted diffusion and internal field gradients. *SPWLA 40th Annual Logging Symposium*, Oslo, Norway, May 30−June 3, 1999; Society of Petrophysicists & Well Log Analysts, 1999; SPWLA-1999-FF.

(44) Kleinberg, R. L.; Horsfield, M. A. Transverse relaxation processes in porous sedimentary rock. *J. Magn. Reson.* **1990**, *88*, 9−19.
(45) Kleinberg, R. L.; Vinegar, H. J. NMR properties of reservoir fluids. *The Log Analyst* **1996**, *37* (06), 20−32.
(46) Li, S.; Guo, H.; Liu, W.; Sun, D.; Li, H. Study on oil saturation recovery on cores by using nuclear magnetic resonance. *J. Oil Gas Technol.* **2007**, *29* (2), 62−66.
(47) Ma, C.; Dong, C.; Lin, C.; Elsworth, D.; Luan, G.; Sun, X.; Liu, X. Influencing factors and fracability of lacustrine shale oil reservoirs. *Mar. Pet. Geol.* **2019**, *110*, 463−471.
(48) Guo, T.; Zhang, S.; Ge, H.; Wang, X.; Lei, X.; Xiao, B. A new method for evaluation of fracture network formation capacity of rock. *Fuel* **2015**, *140*, 778−787.
(49) Liu, H.; Zhang, S.; Song, G.; Xuejun, W.; Teng, J.; Wang, M.; Bao, Y.; Yao, S.; Wang, W.; Zhang, S.; et al. Effect of shale diagenesis on pores and storage capacity in the Paleogene Shahejie Formation, Dongying Depression, Bohai Bay Basin, east China. *Mar. Pet. Geol.* **2019**, *103*, 738−752.
(50) Kleinberg, R. L. Utility of NMR T_2 distributions, connection with capillary pressure, clay effect, and determination of the surface relaxivity parameter ρ_2. *Magn. Reson. Imaging* **1996**, *14* (7−8), 761−767.
(51) Chen, Z.; Lavoie, D.; Malo, M.; Jiang, C.; Sanei, H.; Haeri-Ardakani, O. A dual-porosity model for evaluating petroleum resource potential in unconventional tight shale plays with application to Utica Shale in Quebec, Canada. *Mar. Pet. Geol.* **2017**, *80*, 333−348.
(52) Rouquerol, J.; Avnir, D.; Fairbridge, C. W.; Everett, D. H.; Haynes, J. M.; Pernicone, N.; Ramsay, J. D. F.; Sing, K. S. W.; Unger, K. K. Recommendations for the characterization of porous solids. *Pure Appl. Chem.* **1994**, *66*, 1739−1758.
(53) Hansen, J. P.; Skjeltorp, A. T. Fractal pore space and rock permeability implications. *Phys. Rev. B: Condens. Matter Mater. Phys.* **1988**, *38* (4), 2635−2638.
(54) Krohn, C. E. Fractal measurements of sandstones, shales, and carbonates. *J. Geophys. Res.* **1988**, *93* (B4), 3297−3305.
(55) Jiang, F.; Chen, D.; Chen, J.; Li, Q.; Liu, Y.; Shao, X.; Hu, T.; Dai, J. Fractal analysis of shale pore structure of continental gas shale reservoir in the Ordos Basin, NW China. *Energy Fuels* **2016**, *30* (6), 4676−4689.
(56) Shao, X.; Pang, X.; Li, H.; Zhang, X. Fractal analysis of pore network in tight gas sandstones using NMR method: A case study from the Ordos basin, China. *Energy Fuels* **2017**, *31* (10), 10358−10368.
(57) Jiang, F.; Chen, D.; Wang, Z.; Xu, Z.; Chen, J.; Liu, L.; Huyan, Y.; Liu, Y. Pore characteristic analysis of a lacustrine shale: A case study in the Ordos Basin, NW China. *Mar. Pet. Geol.* **2016**, *73*, 554−571.
(58) Taylor, R. K.; Smith, T. J. The engineering geology of clay minerals: swelling, shrinking and mudrock breakdown. *Clay Miner.* **1986**, *21* (3), 235−2.
(59) Zhao, X.; Pu, X.; Jiang, W.; Zhou, L.; Jin, F.; Xiao, D.; Fu, L.; Li, H. An exploration breakthrough in Paleozoic petroleum system of Huanghua Depression in Dagang Oilfield and its significance. *Petrol. Explor. Dev.* **2019**, *46* (4), 651−663.
(60) Sandvik, E. I.; Young, W. A.; Curry, D. J. Expulsion from hydrocarbon sources: the role of organic absorption. *Org. Geochem.* **1992**, *19*, 77−87.
(61) Behar, F.; Lewan, M. D.; Lorant, F.; Vandenbroucke, M. Comparison of artificial maturation of lignite in hydrous and nonhydrous conditions. *Org. Geochem.* **2003**, *34* (4), 575−600.
(62) Na, J. G.; Im, C. H.; Chung, S. H.; Lee, K. B. Effect of oil shale retorting temperature on shale oil yield and properties. *Fuel* **2012**, *95*, 131−135.
(63) Alpak, F. O.; Vink, J. C.; Gao, G.; Mo, W. Techniques for effective simulation, optimization, and uncertainty quantification of the in-situ upgrading process. *Journal of Unconventional Oil and Gas Resources.* **2013**, *3*, 1−14.
(64) Alpak, F. O.; Vink, J. C. Rapid and accurate simulation of the In-situ Conversion Process using upscaled dynamic models. *J. Pet. Sci. Eng.* **2018**, *161*, 636−656.
(65) Zhao, W.; Hu, S.; Hou, L. Connotation and strategic role of in-situ conversion processing of shale oil underground in the onshore China. *Petrol. Explor. Dev.* **2018**, *45* (4), 563−572.
(66) Zhang, H.; Huang, H.; Li, Z.; Liu, M. Oil physical status in lacustrine shale reservoirs - A case study on Eocene Shahejie Formation shales, Dongying Depression, East China. *Fuel* **2019**, *257*, 116027.
(67) Wang, M.; Guo, Z.; Jiao, C.; Lu, S.; Li, J.; Xue, H.; Li, J.; Li, J.; Chen, G. Exploration progress and geochemical features of lacustrine shale oils in China. *J. Pet. Sci. Eng.* **2019**, *178*, 975−986.
(68) Zhao, X.; Zhou, L.; Pu, X.; Jin, F.; Han, W.; Xiao, D.; Chen, S.; Shi, Z.; Zhang, W.; Yang, F. Geological characteristics of shale rock system and shale oil exploration breakthrough in a lacustrine basin: A case study from the Paleogene 1st sub-member of Kong 2 Member in Cangdong sag, Bohai Bay Basin, China. *Petrol. Explor. Dev.* **2018**, *45* (03), 377−388.

https://dx.doi.org/10.1021/acs.energyfuels.0c03978
Energy Fuels 2021, 35, 2209−2223